Nanoscale

ROYAL SOCIETY OF CHEMISTRY

PAPER

View Article Online
View Journal | View Issue

Cite this: *Nanoscale*, 2024, **16**, 22411

pH controlled synthesis of end to end linked Au nanorod dimer in an aqueous solution for plasmon enhanced spectroscopic applications†

Shubhangi Sharma,[a] Théo Minchella,[b] Susmita Pradhan,[a] Davy Gérard,[b] Quanbo Jiang[b] and Satyajit Patra *[a]

End-to-end linked nanorod dimer nanogap antennas exhibit superior plasmonic enhancement compared to monomers due to the coupling of localized surface plasmon resonances (LSPR) of individual nanorods. However, controlling the assembly to stop at the dimer stage is challenging. Here, we report a pH-controlled synthesis of Au nanorod dimer nanogap antennas in an aqueous solution using 1,4-dithiothreitol (DTT) as a linker. Neutral to acidic pH (4.0 to 7.0) favors dimer formation, while higher pH decreases dimer yield, stopping completely at pH 11.0. The reaction can also be halted in neutral and acidic solutions by abruptly increasing the pH to 11.0 or higher. At basic pH, both thiol groups of DTT deprotonate and acquire a negative charge, causing both thiolate ends to adsorb onto the positively charged cetyltrimethylammonium bromide (CTAB) micellar layer on the transverse surface of the Au nanorod, preventing dimer formation. TEM images confirm nanorod dimers, showing a good conversion yield (~80%) from monomers to dimers. Overall, out of all the DTT induced NR assemblies, 70% are found to be dimers. The majority of these dimers (>90%) are end-to-end linked dimers, with a gap distance of ~1 nm, exhibiting exceptional stability and remaining intact for over two weeks. FDTD simulations demonstrate a significant enhancement of the light E field in the nanogap, ~80 times higher than in a homogeneous water environment and 11 times higher than in nanorod monomers. Simulations also show that E field enhancement varies with the angular separation of monomeric nanorods, being highest for end-to-end dimers (180°) and lower for side-to-side dimers (0°). Overall, we present an inexpensive method to design and control nanorod dimer nanogap antennas in aqueous solution, useful for plasmon-enhanced spectroscopic applications such as biosensing, chemical sensing, and biomedical devices.

Received 6th August 2024,
Accepted 3rd November 2024

DOI: 10.1039/d4nr03235g

rsc.li/nanoscale

1. Introduction

Controlling and manipulating light at the nanoscale, far below the diffraction limit, opens up new opportunities. These include developing optical methods for detecting molecules beyond the diffraction barrier, designing high-resolution biosensing and chemical sensing assays that can lower the limit of detection (LOD) for target analytes, biomedicine, catalysis and creating optical circuits that can harvest, modulate, and reemit light at the nanoscale.[1,2,3–10,11–16] This control and manipulation of light at the nanoscale, beyond the diffraction limit, is made possible through the coupling of light with the localized surface plasmon resonance (LSPR) of plasmonic nanostructures, such as those made of gold (Au), silver (Ag), and aluminum (Al). This interaction leads to a significant enhancement of the electric field (E-field) in the vicinity of the plasmonic nanostructures, known as a hot spot. When an emitter is placed in the hot spot, the enhanced light–matter interaction results in an emission signal that is several orders of magnitude higher compared to the absence of plasmonic nanostructures.[2,17–20] This enhances the spatial and temporal resolution of existing spectroscopy and microscopy techniques (*e.g.*, Raman and fluorescence), allowing the study of biological and chemical processes at timescales not accessible with conventional spectroscopy techniques.[19,21,22] Key to these applications is the generation of intense electromagnetic hotspots near the metal nanostructures. It has been observed that an assembly of two or more metal nanoparticles (NPs) in close proximity generates intense electromagnetic hotspots in the nanogap, with electric field enhancements 2–3 orders of magnitude higher compared to isolated metal NPs.[23–26] This is due to the coupling of the LSPR of the individual metal NPs in the assembled structure, creating a hybrid plasmon mode[27] that

[a]*Birla Institute of Technology and Science-Pilani, Pilani campus, Pilani-333031, Rajasthan, India. E-mail: satyajit.patra@pilani.bits-pilani.ac.in*
[b]*Light, Nanomaterials, Nanotechnologies (L2n) Laboratory, CNRS UMR 7076, University of Technology of Troyes, 12 rue Marie Curie, 10004 Troyes, France*
† Electronic supplementary information (ESI) available. See DOI: https://doi.org/10.1039/d4nr03235g

results in huge near-field light enhancement and an increase in the local density of optical states (LDOS) in the gap of these nanostructures.[23,28,29] An assembly of anisotropic metal NPs exhibits even superior plasmonic enhancement compared to their isotropic counterparts due to sharp tips that lead to tighter confinement of light and more intense electromagnetic hotspots.[3,18,30–32] Among these anisotropic NP assemblies, nanorod (NR) assemblies are the most popular. This is because NRs can be easily prepared in large quantities in a reproducible manner using wet chemical synthesis, and their LSPR band can be tuned to the desired wavelength by simply changing the aspect ratio.[33–37] Khatua and colleagues observed over 10 000-fold enhancements in the fluorescence of a single molecule for an end-to-end assembly of an Au NR network.[38] Lu *et al.* observed a 10^8-fold enhancement in two-photon excited fluorescence of a single ATTO 610 dye in the gap of a dimer NR.[39] Zhang *et al.* found a 470-fold increase in single-molecule fluorescence in the 6.1 nm gap of a dimer NR.[40] Therefore, NR dimers remain very attractive materials for plasmonic-enhanced spectroscopic applications.

There are generally two methods used to fabricate assemblies of metal nanostructures: top-down lithography and bottom-up wet chemical synthesis. Top-down techniques, such as focused ion beam (FIB) and electron lithography, create nanostructures with precise size, shape, and gap distances at high resolution and reproducibility.[28] However, these methods are extremely costly and result in polycrystalline nanostructures, causing plasmonic losses at grain boundaries.[41] In contrast, bottom-up wet chemical synthesis has made significant progress over the past two decades in fabricating anisotropic metal nanostructures with high reproducibility.[42,43] This method is inexpensive and can be used in any experimental lab. It also produces single-crystalline nanomaterials with superior plasmonic properties compared to those formed by top-down lithography. Various groups have developed different strategies to prepare end-to-end assemblies of Au nanorods (NRs) using wet chemical synthesis. For example, Jain *et al.* used a seed-mediated growth approach to anisotropically grow dimerized Au nanoseeds into end-to-end Au NRs.[44] Murphy and co-workers employed biotin–streptavidin interactions to create highly ordered arrays of end-to-end Au NRs.[45] The Thomas group utilized alkane dithiol in acetonitrile to synthesize end-to-end Au NR assemblies, where the dithiol binds specifically to the NR tips due to the lower density of CTAB in these regions.[46,47] Liu *et al.* used dithiol polyethylene glycol (HS-PEG-SH) to create both end-to-end and side-by-side assemblies of Au nanorods (NRs).[48] They found that at lower concentrations, HS-PEG-SH favors end-to-end assembly, while at higher concentrations; it promotes side-by-side assembly. Hemant *et al.* have prepared a μm long end to end assembly of Au NRs using a linear diamino derivative of BODIPY as a linker.[49] Complementary oligonucleotide hybridization has also been used to synthesize end-to-end NR assemblies.[40] Although these studies achieved high yields for end-to-end NR assemblies, they lacked control to stop the assembly reaction at the dimer stage. While DNA origami can create NR dimers with precise gap distances, this method is tedious and expensive.[50–53]

Recent efforts have focused on stopping the assembly reaction at the dimer stage through more affordable routes. Lu *et al.* employed a physical technique where the reaction solution was deposited between two glass slides, allowing the excess NRs to drain away, thus stopping the assembly reaction.[54] However, this method lacks chemical control over the assembly reaction. Nepal *et al.* prepared a highly stable side-to-side linked Au NR dimer in an ethanol-water mixture by modulating directional interactions through the depletion and reassembly of the CTAB bilayer on the sides of the Au NRs.[55] However, the plasmonic enhancement in the side-to-side linked NR dimer is much lower compared to the end-to-end linked dimer.[56] Lecaque and colleagues utilized hydrogen bonding between the carboxylate group and the protonated amine group of two distinct cysteines to form an end-to-end assembly of Au NRs, which could be halted at the dimer stage by adding $AgNO_3$.[57] The NR dimers prepared using this method remained stable for only 24 hours. The same group also used the bifunctional coupling agent *trans*-1,2-bis (4-pyridyl) ethylene (BPE) to link the ends of Au nanorods. The reaction was stopped at the dimer stage with $AgNO_3$, and the dimers were encapsulated in mesoporous silica for long term stability.[58,59] Stewart *et al.* tethered thiolated polystyrene to the ends of gold nanorods (Au NRs) to promote end-to-end assembly through hydrophobic interactions.[60] They used phospholipid encapsulation to halt the assembly at the dimer stage and to provide stability to the NR dimer. The use of an encapsulation layer around the NR, however, may limit access to the electromagnetic hotspot, as the plasmonic near field decays exponentially from the surface of the NRs.[61] This could hinder plasmonic-enhanced spectroscopic applications. Therefore, it is important to prepare a solution-stable, end-to-end linked Au nanorod dimer without an encapsulation layer. Recently, Khatua and colleagues used the pH-sensitive properties of poly (acrylic acid) (PAA) to halt the Au NR assembly at the dimer stage in acetonitrile.[62,63] They used PAA-coated Au NRs and 1,6-hexane dithiol as a linker. The reaction was stopped by increasing the pH with DABCO, deprotonating the PAA's COOH groups, which made the NRs negatively, charged and prevented further binding. This method achieved almost 60% dimer yield, with dimers remaining stable for about seven days after adding high concentrations of DABCO. However, since 1,6-hexane dithiol is not soluble in aqueous medium, this method is not suitable for biological applications requiring NR dimers in aqueous solutions. Additionally, PAA-coated Au NRs tend to aggregate in acetonitrile due to poor solubility. Therefore, an alternative strategy is needed to prepare Au NR dimers in aqueous medium.

We have used 1,4-dithiothreitol (DTT) to prepare end-to-end dimers with a gap distance of ~1 nm in aqueous solution. Previously, Tsai *et al.* employed DTT to link spherical Au nanoparticles, forming clusters in water.[64] They further stabilized the DTT-conjugated nanoparticles by attaching thiolated polyethylene glycol (PEG-SH), which prevented further aggregation

through steric repulsion. However, no anisotropic nanoparticles, such as NRs, were linked end-to-end, and no *in situ* control was applied to stop the reaction at the dimer stage. In the present study, DTT is used to link the two Au NRs to prepare an end to end dimer. The reaction can be easily controlled by adjusting the pH. Dimer formation is more favorable at acidic and neutral pH but becomes less favorable as pH increases, stopping completely at pH ≥ 11.0. The reaction can also be halted at neutral and acidic pH by rapidly increasing the pH to 11.0. At high pH (≥11.0), both SH groups of DTT deprotonate and acquire a negative charge, adsorbing onto the positively charged cetyl trimethyl ammonium bromide (CTAB) micellar layer on the transverse surface of the Au NRs, making them unavailable to bind with another NR. We found that the nanorods prepared using this method, are stable for over two weeks. Finite-difference time-domain (FDTD) simulations reveal a significant enhancement of the electric field at the gap of the dimer nanorod. Additional FDTD simulations indicate that the electric field enhancement is maximum in a linear end-to-end dimer configuration and lowest in a side-to-side dimer configuration. Overall, we have developed a cost-effective strategy to prepare Au NR dimers in aqueous solution, which will be useful for various plasmon-enhanced spectroscopic applications, including biochemical sensing and photovoltaic devices.

2. Experimental section

2.1. Materials

Chloroauric acid trihydrate ($HAuCl_4{\cdot}3H_2O$), cetyltrimethylammonium bromide (CTAB), L-ascorbic acid, silver nitrate ($AgNO_3$), 1,4 dithiothreitol (DTT), hydrochloric acid (HCl), potassium hydroxide (KOH), acetic acid were all purchased from Sigma Aldrich (Merck) and were used as received. MilliQ water was used in all the experiments.

2.2. Preparation of Au nanorods (NRs)

Au nanorods were prepared using the seed-mediated growth approach.[33,35,37] First, Au nanoseeds were prepared in an aqueous solution by reducing $HAuCl_4$ (25 μL of 50 mM $HAuCl_4$) in CTAB (4.7 mL, 0.1 M) using a freshly prepared ice-cold solution of $NaBH_4$ (300 μL, 10 mM) under vigorous stirring at 30 °C for 2 minutes. The solution color changed from yellow to brown within 30 s confirming the formation of the Au nanoseed. Next, the Au nanoseed solution was aged at 30 °C for 1 h. After then, the Au nanoseeds were anisotropically grown into nanorods (NRs) in a growth medium containing $HAuCl_4$, CTAB, HCl, and ascorbic acid at 30 °C. To prepare this growth solution, 190 μL of 1 M HCl and 100 μL of 50 mM $HAuCl_4$ were added to 10 mL of 0.1 M CTAB solution and stirred gently for 5 minutes. The final pH of the solution was 1.8. Then, 120 μL of 10 mM $AgNO_3$ was added under mild stirring. After that, 100 μL of 100 mM ascorbic acid was mixed in, turning the solution from yellow to colorless, indicating the reduction of Au^{3+} to Au^{1+}. Finally, 24 μL of the aged Au nanoseed solution was added, and the mixture was left undisturbed overnight (~12 h). The solution turned deep red, indicating the formation of Au NRs. To remove excess CTAB, the Au NR solution was centrifuged at 10 000 rpm, and the NRs were redispersed in Milli-Q water for storage and further use.

2.3. Preparation of end to end linked Au nanorods (NRs)

End to end linked Au NRs were prepared by linking the Au NR monomers using the linker 1,4-dithiothreitol (DTT). DTT has two thiol (–SH) groups which provides two anchoring motif to bind with two monomeric Au NRs. The assembly reaction was performed in aqueous medium at different pH (4 to 11). To obtain the desired pH, necessary concentration of acetic acid and KOH were added into the reaction mixture. For all the measurements the optical density of the Au NR solution was fixed at 0.3 to 0.4. First, a 600 μL aqueous solution of the Au NR monomer was taken in a cuvette (volume-700 μL, path length 0.2 cm, Starna) and to this 30 μL of 50 mM DTT was added and the solution was mixed properly. The progress of the reaction was monitored in a UV-Vis-NIR spectrophotometer (Lambda 1050+, PerkinElmer) as a function of time at different time interval. The decrease of the LSPR band of the Au NRs and the appearance of a new band at NIR (>950 nm) indicates the formation of end to end linked Au NRs. The reaction can be stopped at the dimer stage before the isosbestic point is lost by a sudden increase of pH of the medium. To increase the pH of the medium from 4.0 to 11.0, ~1.5 μL of 5 M KOH was added into the reaction mixture and mixed thoroughly.

2.4. Transmission electron microscopy (TEM)

TEM measurements were conducted at two different locations. At the Central Research Facilities, IIT Delhi, Sonipat campus, a 200 kV high-resolution transmission electron microscope (JEM-ARM200F NEOARM) was used. Additionally, TEM images were obtained at the Central Research Facilities, MNIT Jaipur, using a 200 kV Tecnai G2 20 S-TWIN (FEI) microscope. The TEM samples were prepared by drop-casting the sample onto carbon-coated copper grids with a 400 mesh size.

2.5. Zeta potential measurements

Zeta potential measurements were conducted on a Litesizer-500 (Anton Paar) using a univette low volume cuvette (60 μL). The measurements were conducted in water at different pH at 25 °C.

2.6. Absorption spectroscopy measurements

Absorption spectra of Au NRs were conducted in a UV-Vis-NIR spectrophotometer (Lambda 1050+, PerkinElmer) cuvette (volume-700 μL, path length 0.2 cm, Starna). The optical density of Au NRs was kept at 0.3–0.4 by dilution. The absorption spectra are taken at different time intervals to monitor the progress of the end to end assembly reaction. All the measurements were conducted at 25 °C.

2.7. Finite difference time domain (FDTD) simulation

FDTD simulations were conducted on a commercial software Ansys Lumerical. Two different meshes were used: a 1 nm

mesh surrounding the dimers, as well as a 0.5 nm mesh near the gaps. Total Field Scattered Field (TFSF) illuminates the NR dimers as a planar source at 1030 nm, with polarisation along the *x*-axis. The NR dimers are made of gold, by taking the complex refractive index from Johnson & Christy into account, in suspension in the water medium. The geometry of each NR monomer is defined as a cylinder with two half-spheres ends, which gives results closer to the reality as well as allowing NR dimers to rotate while keeping a constant gap size. The length and diameter of each NR monomer are 45 nm and 15 nm respectively. The maps of electric field enhancements were obtained by normalizing the electric field in the presence of Au NRs with respect to the electric field in absence of any Au NRs. To compare the values of electric field enhancements between angles, a 2D square monitor (*z* normal) is placed in the gap, with side equal to the gap size. We compare the mean value of electric field enhancements in the monitor, to limit numerical artefacts influence.

2.8. Scanning tunnelling electron microscopy (STEM) imaging measurements

STEM images were acquired using an FEI Apreo S LoVac scanning electron microscope. The samples were prepared by drop-casting Au NRs onto a carbon-coated copper grid with a 400-mesh size and air-dried overnight.

3. Results and discussion

3.1. pH controlled end to end assembly of Au nanorods (NRs)

The end-to-end assembly of Au nanorods (NRs) is prepared using the linker 1,4-dithiothreitol (DTT) in an aqueous solution, as detailed in the Experimental section. DTT has two thiol (–SH) groups, which can bind to two Au NRs to form end-to-end linked Au NR dimers (Fig. 1A). The TEM images of Au NR monomers are shown in Fig. S1 (ESI).† The Au NRs have dimensions of 40 ± 5 nm in length and 15 ± 5 nm in width. DTT binds to the tip region of the Au NRs due to the low density of CTAB in this area (Fig. 1A). The assembly reaction is monitored over time by recording the absorption spectra at different time intervals. The absorption spectra of Au NRs as a function of time at pH 4.0 are provided in Fig. 1B. We observed that the optical density of the Au NRs at the localized surface plasmon resonance (LSPR) wavelength decreases with increasing time, coinciding with the appearance of a new band at $\lambda >$ 940 nm, indicating the formation of Au NR dimers. An isosbestic point appears at 912 nm. The new band in the near-infrared (NIR, $\lambda >$ 940 nm) region arises due to the coupling of the LSPR of the individual monomeric Au NRs, resulting in the formation of a hybrid plasmon mode, which is lower in energy than the individual Au NRs and thus red-shifted compared to the LSPR band.[23,28,56,65] After 150 minutes, the isosbestic

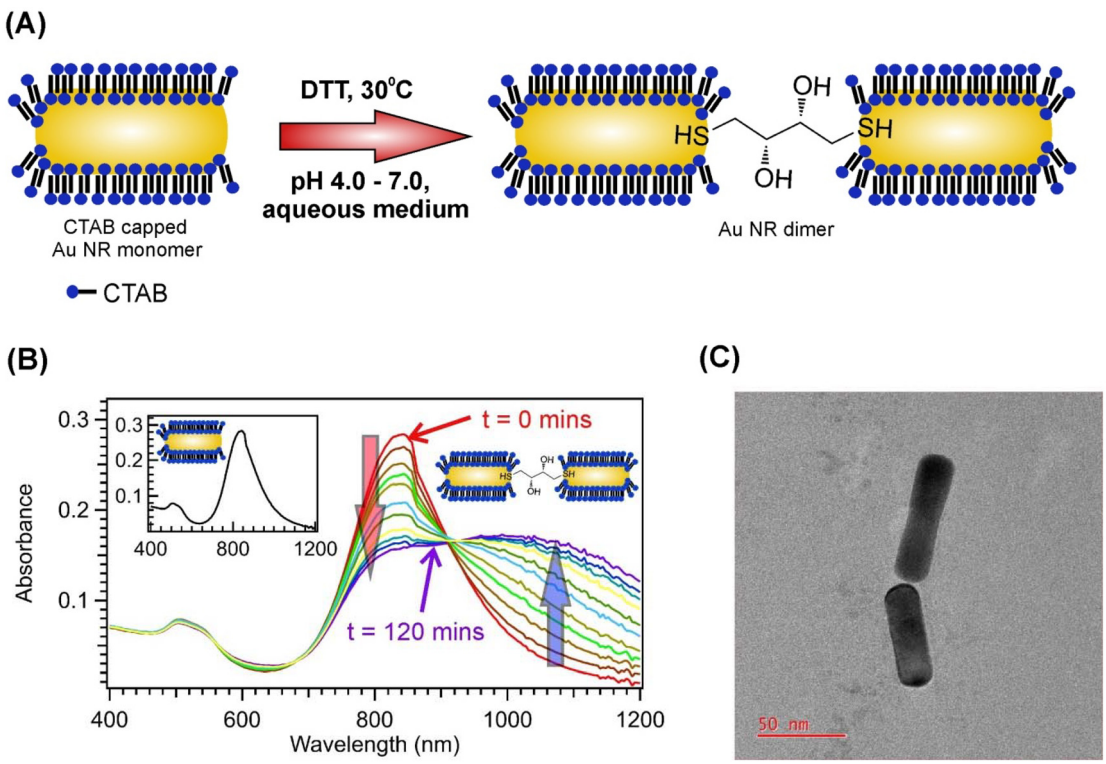

Fig. 1 Preparation and characterization of Au NR dimer. (A) Schematic presentation of the Au NR dimer preparation from the Au NR monomer using the 1,4-dithiothreitol (DTT) as a linker in aqueous medium. (B) Absorption spectra as a function of time which monitor the progress of the dimer reaction over time in aqueous medium at pH 4.0. (C) Transmission electron microscopy (TEM) image of an Au NR dimer with a gap size ~1 nm.

point is lost (Fig. S2, ESI),† and the assembly reaction leads to the formation of higher-order multimeric structures, such as trimers and tetramers (Fig. S3, ESI†). To further confirm that the linkage between the NRs is due to DTT, we record the absorption spectra of Au NRs over time at pH 4.0 without DTT (Fig. S4, ESI†). We observe no changes in the absorption spectra, indicating that DTT is essential for linking the NRs. The TEM samples for imaging the Au NR dimers are prepared by drop-casting the reaction solution onto carbon-coated Cu grids and drying them before the isosbestic point is lost. The TEM images confirmed the formation of end-to-end linked Au NR dimers (Fig. 1C).

Next, we have investigated the pH sensitivity of the assembly reaction. The absorption spectra with time for the assembly reactions at different pH are shown in Fig. 2. Necessary amount of acetic acid and KOH is added into the aqueous solution of Au NRs to obtain the desired pH. We found that the deceases in the absorbance at LSPR and rise in absorbance at NIR (λ > 900 nm) with time is more prominent for neutral and acidic pH (Fig. 2A and B) and as the pH increases this decrease at LSPR and rise at NIR decreases considerably (Fig. 2C) and at pH 11.0, there is hardly any change in the absorption spectra with time (Fig. 2D). The results indicate that the assembly reaction is more prominent at neutral and acidic pH and the reaction yield decreases with increasing pH and at pH 11.0 the reaction completely stops. Next, we have determined the amplitude and rate of the end to end assembly reaction of the Au NRs at different pH to obtain more insights into the influence of pH on the assembly reaction. Normalized plot of the absorbance at LSPR of the Au NRs as a function of time at different pH is shown in Fig. 3A. These plots are fitted to a monoexponential function, $A = A_0 + R\exp(-kx)$, where, A is the absorbance at any given time t, A_0 is the residual absorbance *i.e.* when the reaction gets saturated, R is the amplitude of the reaction and k is the rate constant. The plot of amplitude and rate constant of the reaction is provided in Fig. 3B and C, respectively. The amplitude of the reaction decreases from 64% at pH 4.0 to 33% at pH 7.0, 22% at pH 9.0, and 8% at pH 11.0. The rate constant, k of the reaction remain more or less same at 0.01 min^{-1} from pH 4.0 to 9.0 but decreases drastically to 0.002 min^{-1} at pH 11.0. However, the small decrease in the absorbance at LSPR of the Au NRs observed at pH 11.0 (Fig. 3C) is possibly not due to the assembly reaction as no rise is observed at the NIR range and this is most probably arises due to surface reconstruction and adsorption of negatively charged DTT on the positively charged CTAB layer on the transverse surface of the Au NRs. From these results it is quite evident that the end to end assembly reaction of the Au NRs is sensitive to pH and hence, can be controlled by adjusting pH of the aqueous solution.

3.2 pH jump experiment and mechanism behind the pH sensitivity of the end to end assembly reaction

We also aimed to control the reaction to stop at the dimer stage *in situ*, preventing progression to higher-order clusters (*e.g.*, trimers, tetramers, polymers, *etc.*). To achieve this, we performed a pH jump study where the pH of the reaction medium was suddenly increased by adding the necessary

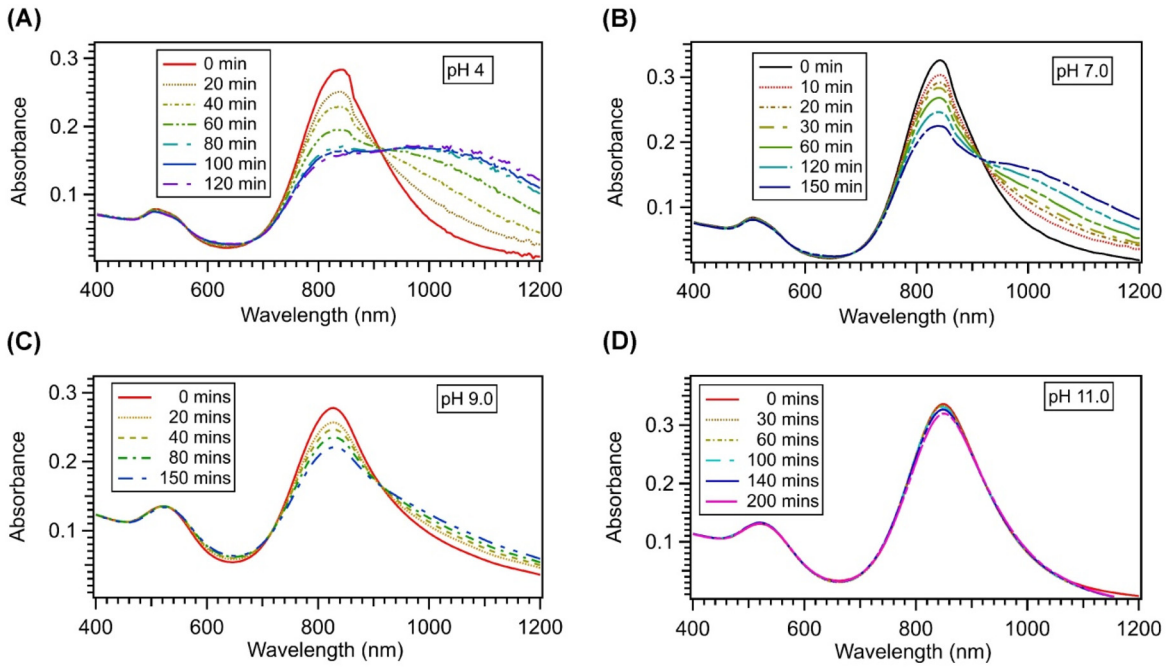

Fig. 2 pH sensitivity of the end to end assembly of the Au NRs. Absorption spectra at different times after the addition of DTT monitoring the progress of the reaction at (A) pH 4.0, (B) pH 7.0, (C) pH 9.0, and (D) pH 11.0 respectively. With increasing pH the extent of the reaction decreases and at pH 11.0 the reaction completely stops.

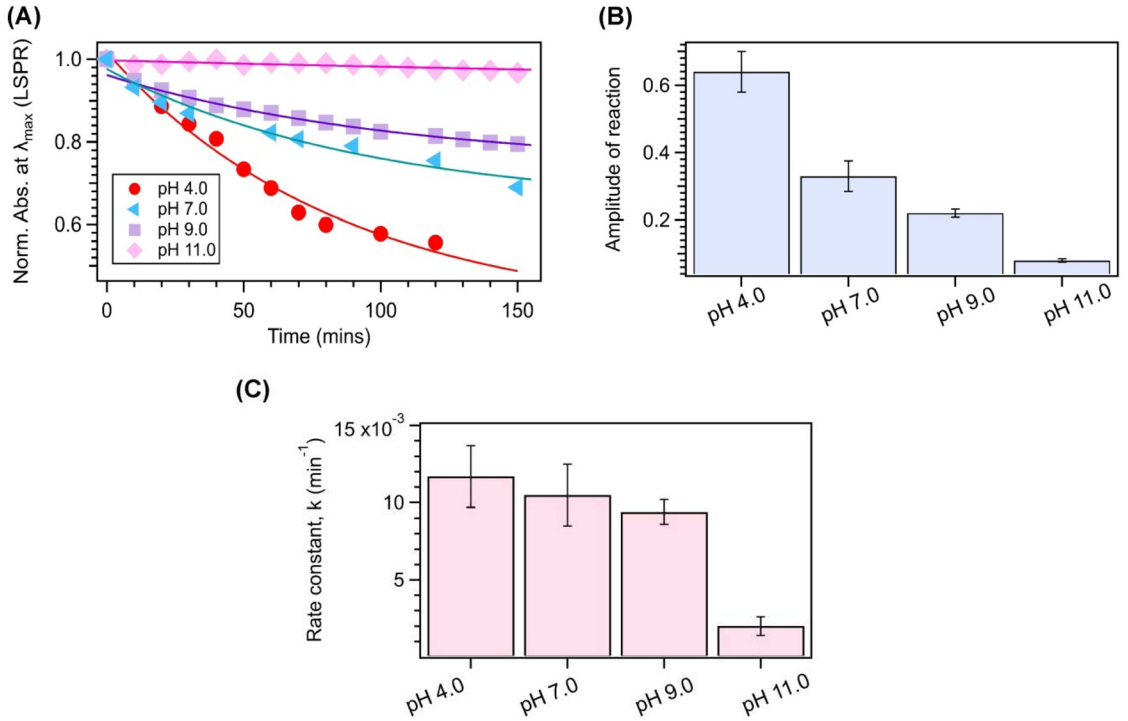

Fig. 3 Amplitude and rate of the assembly reaction as a function of pH. (A) Plot of normalized absorbance at LSPR of the Au NRs as a function of time in aqueous solution for different pH. Here, symbols are the data and line is the monoexponential fit to the data. Plot of amplitude (B) and rate constant (C) of the assembly reaction as a function of pH.

amount of KOH during the course of the reaction. This stops the reaction at the dimer stage. Fig. 4A shows the absorption spectra of the Au NRs in the assembly reaction obtained from the pH jump experiment. We started the assembly reaction in an aqueous medium at pH 4, and then, before the isosbestic point was lost, at 50 minutes, we added KOH to increase the pH from 4 to 11. From the absorption spectra, we can see that before adding KOH, the absorbance of the Au NRs at LSPR gradually decreases from 0.28 to 0.22. However, after adding KOH, the absorbance remains more or less constant at 0.22 (Fig. 4A). We plotted the absorbance value as a function of time to determine the rate constant before and after the addition of KOH (Fig. 4B). The rate constant before adding KOH was found to be 0.0090 ± 0.0015 min^{-1}, and after adding KOH, it was 0.0020 ± 0.0005 min^{-1} (Fig. 4C). Therefore, the results clearly show that we can control the end-to-end assembly of the Au NRs by increasing the pH of the reaction medium. After KOH addition, the NR dimers remain stable for at least two weeks, with minimal changes in the absorption spectra (Fig. S5A, ESI†). STEM images confirm that most of the structures remain as NR dimers after two weeks (Fig. S5B, ESI†).

Next, we aimed to understand the mechanism behind the pH sensitivity of the end-to-end linked Au NRs assembly reaction. To do this, we first conducted zeta potential measurements to determine the surface charge of the Au NRs at different pH levels. Fig. 5A shows the results of these measurements. The zeta potential value decreases from +59.86 mV at pH 4.0 to +30.32 mV at pH 11.0, but it remains positive even at basic pH, indicating that the Au NRs surface charge is still positive at higher pH levels. After determining the surface charge of the Au NRs, we focused on understanding the behavior of DTT at different pH levels. DTT has two thiol groups, with its first and second pK_a values being 8.9 and 10.3, respectively.[66] At pH 8.9, 50% of the DTT has one thiol group deprotonated, making it monoanionic. At pH 10.3, 50% of DTT has both thiol (–SH) groups deprotonated, making it dianionic (Fig. 5B). The surface of the Au NRs, particularly at the transverse surface, is positive due to the high density of the positively charged CTAB micellar layer. At pH 11, when DTT becomes dianionic, both thiolate (S^-) ends of the DTT bind to the CTAB micellar layer on the transverse surface of the Au NRs, preventing it from binding with another Au NR, thus stopping the reaction (Fig. 5D). At pH 9, most of the DTT is in monoanionic form, and it adsorbs onto the CTAB-rich transverse surface through electrostatic interaction. However, it is unlikely for the remaining neutral -SH group of the monoanionic DTT to bind with another NR due to the strong electrostatic repulsion from the CTAB micellar layer (Fig. S6, ESI†). This results in a lower reaction yield for the Au NR assembly reaction at pH 9.0 due to the lower population of neutral DTT molecules. At pH 4.0 and 7.0, DTT is in neutral form with two available –SH groups, which can bind to two Au NRs at the tip regions and facilitate end-to-end linking of the Au NRs (Fig. 5C). As the pH increases, more DTT becomes negatively charged and binds to the positively charged CTAB micellar

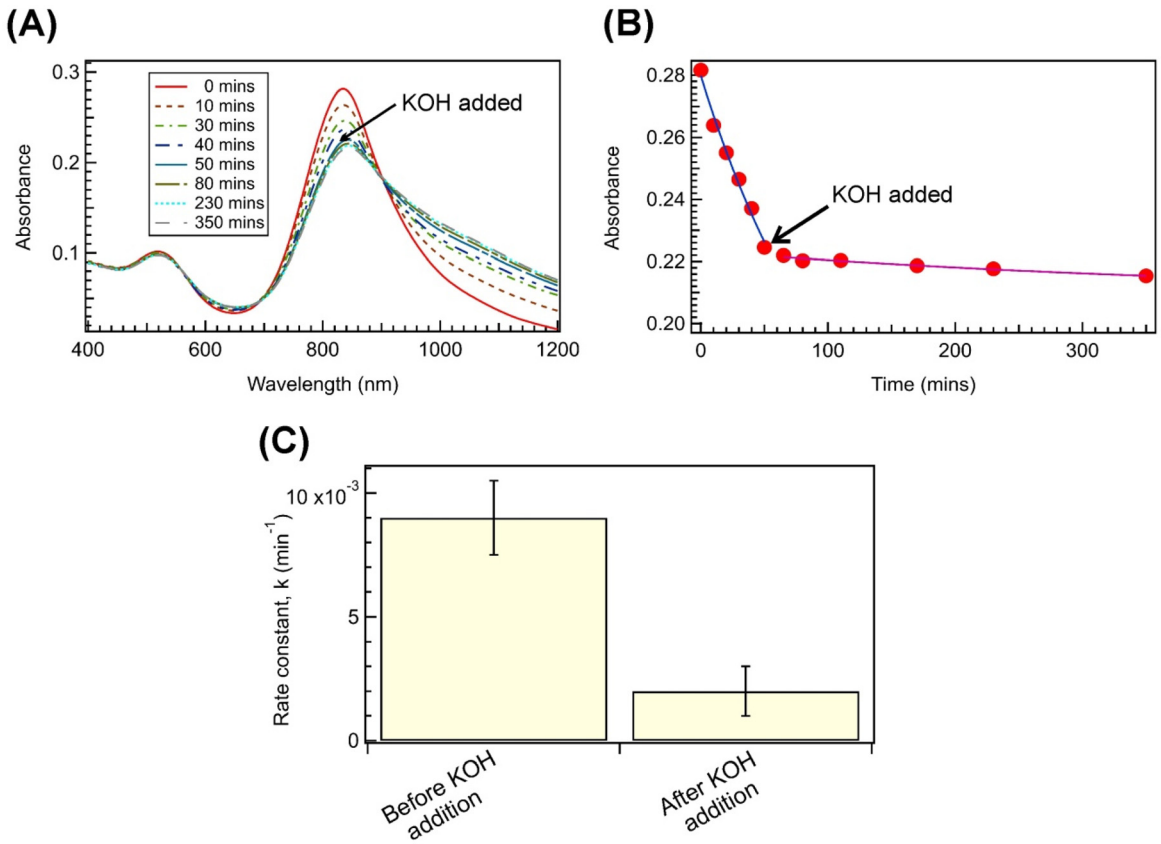

Fig. 4 Results of the pH jump experiment. (A) Absorption spectra of the Au NRs at different times obtained in the pH jump experiment. At 50 minutes during the course of the reaction desired amount of KOH is added in the reaction medium to increase the pH from 4 to 11. (B) Plot of absorbance at λ_{max} as a function of time. The time when KOH is added is shown by the arrow. (C) Bar plot showing the rate constant, *k* values before and after the addition of KOH.

layer on the transverse surface, gradually decreasing the extent of the reaction. At pH 11, nearly the entire population of DTT becomes dianionic, readily adsorbing onto the transverse surface of Au NRs rich with the positively charged CTAB micellar layer, making it unavailable to bind with other NRs and stopping the reaction. Therefore, the acid–base chemistry of DTT provides an easy and elegant approach to control the end-to-end linking of the Au NRs at the dimer stage.

3.3. Conversion yield of monomer to nanoaggregates and dimer counts

After investigating the absorbance data at different pH, we focused on obtaining the overall conversion yield of the monomer to assembled structures. The TEM images of the end-to-end assembly of the Au NRs are shown in Fig. 6A and B. These images clearly show the formation of the Au NR assemblies, including dimers, trimers, and clusters. The gap distance between the NRs in the NR assembly, determined to be 0.7 to 1.0 nm, is very close to the molecular length of DTT (Fig. S7, ESI†). The conversion yield of monomers to assembled structures was calculated by determining the ratio of monomer units forming dimers/clusters to free monomer units. We found that almost 80% of the Au NR monomers converted into assembled structures (dimers, trimers, and clusters). We also counted the total number of dimers, trimers, and clusters from a pool of 200 nanoparticles. The occurrence histogram is shown in Fig. 6C. We observed that 46% of these particles are dimers, 13% are tetramers/clusters, and 5% are trimers. This gives a total of 128 assembled particles, of which 92 are dimers; meaning 71.9% of the assembled structures are dimers.

Due to the flexibility of the DTT linker, the Au NR dimers exhibit a range of angular distributions between the component Au NR monomers (Fig. 6B). The statistical distribution of the angle between the Au NRs in the dimer structures is shown in Fig. 6D. The most probable angle between the Au NRs in the dimers ranges from 60° to 120°. Most of the dimers are formed by end-to-end linking of the Au NRs, and only 7% of the dimers are formed *via* side-to-side coupling (θ = 0°). Thus, this method not only allows us to obtain a high yield of dimers over other assembled structures, but also ensures a high yield of end-to-end coupling between the Au NRs.

3.4. FDTD simulation studies

FDTD simulations were performed to analyse the electric field enhancement due to plasmonic resonance of Au NR dimers.

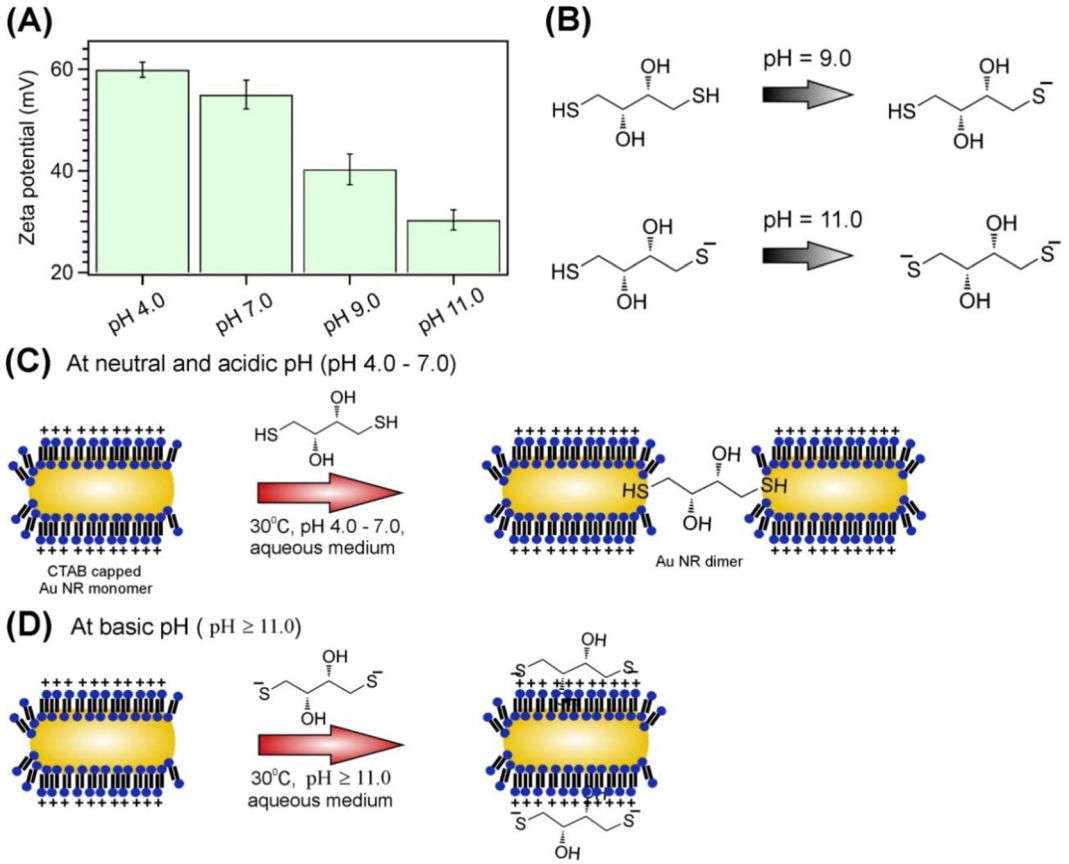

Fig. 5 Mechanism of the pH controlled synthesis of end to end linked Au NR dimers. (A) Bar plot showing the zeta potential of Au NRs as a function of pH. (B) Schematics of the acid base chemistry of DTT at pH 9.0 and 11.0 respectively. (C) Graphical presentation of the end to end linking of Au NRs using DTT as a linker at neutral and acidic pH (pH 4.0 to 7.0). (D) Schematics of the reaction at pH ≥ 11.0.

The maps of electric field enhancements in the vicinity of the NR dimers (45 nm in length and 15 nm in diameter) with gap sizes varying from 1 nm to 20 nm are shown in Fig. 7A–E. It turns out that smaller gap sizes lead to higher electric field enhancements in the gap following with an exponential decay of the electric field as a function of gap size (Fig. 7F). The NR dimers with 1 nm gap size shows 11 fold higher electric field enhancement than the case with NR monomer (the inset of Fig. 7F) while around 80 times higher electric field enhancement than the case without NRs in a homogeneous aqueous environment. When the gap between the two arms of the nanorod dimers is smaller, the coupling of the plasmons is stronger. This results in a higher local density of optical states (LDOS) and greater electric field enhancement in the gap of the nanorod dimer. As the gap between the nanorods (NRs) increases, the plasmon coupling weakens, leading to lower LDOS and less electric field enhancement in the gap. When the gap between the two arms of the NRs is 15 nm or more, the plasmon coupling nearly disappears, and the NR dimer behaves like an isolated gold nanorod (Fig. 7D–F).[29,67,68]

The simulations also predict the maps of electric field enhancements when the angular separation of monomeric NRs is varying. In our simulation, the inter-rod angle refers to the angle formed by the longitudinal axes of the two arms of the NR dimer (inset Fig. 6D). We fixed the orientation of one NR monomer (one arm of the NR dimer) always parallel to the direction of light polarization *i.e.* along the x axis, while the orientation of the other NR monomer is varying to vary the inter-rod angle. The angle of side-to-side dimers in Fig. 8A is defined as 0°. The second arm of the NR dimer opens gradually while the distance of gaps is always kept 1 nm (Fig. 8A–E) until the end-to-end dimer with the angle of 180° is reached. It turns out that the electric field enhancement increases with increasing angles from 0° to 180° (Fig. 8F) which is consistent with the literature reports.[56] At an inter-rod angle of 60°, the electric field enhancement is more than 30 times higher than without NRs. According to the angular distribution of NR dimers from TEM in Fig. 6D; most dimers have angles greater than 60°. This suggests that, using our synthetic approach, we can produce NR dimers that enhance the electric field in the gap at least 30 times higher than in homogeneous water without nanostructures. Moreover, dimers with angles greater than 100° show a 60-fold increase in electric field enhancement (Fig. 8C), reaching a maximum at a 180° angle where the enhancement is ~80 times higher than the homogeneous

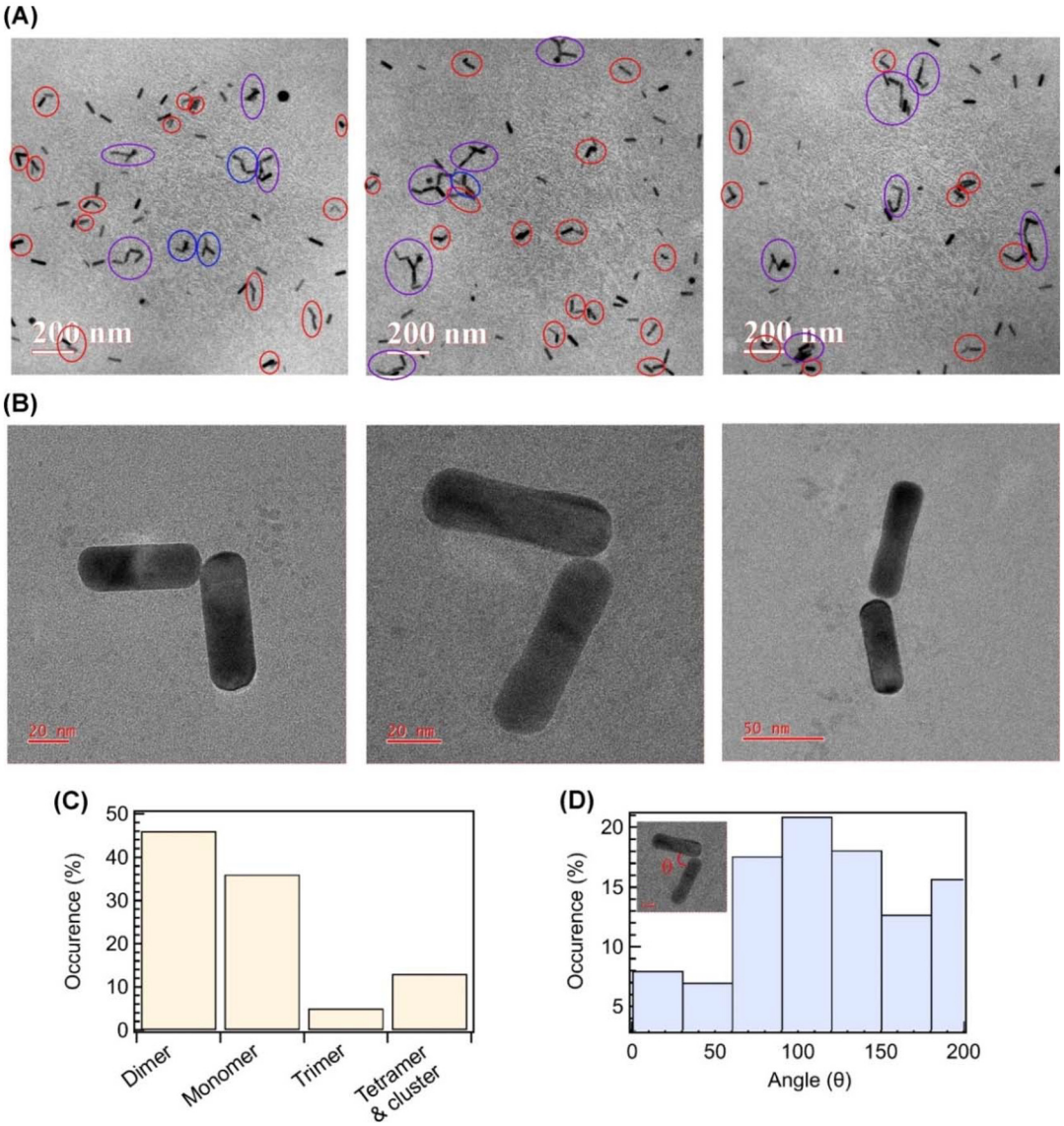

Fig. 6 Structural characterization of the Au NR dimers. (A) Transmission electron microscopy (TEM) image showing the assembly of Au NRs at lower magnification (200 nm scale). Red circles indicate dimers, blue circles indicate trimers, and violet circles indicate tetramers/clusters. (B) Higher magnification TEM images of individual Au NR dimers. (C) Bar plots showing the percentage distribution of different particles: monomers, dimers, trimers, and tetramers/clusters. A total of 200 particles were analyzed. (D) Bar plot showing the angular distribution of the two Au NRs in the Au NR dimers. A total of 92 dimers were analyzed.

water reference (Fig. 8E). So, overall we have high quality NR dimers that will give us electric field enhancement in the gap 30 times higher or more which will be very useful for plasmonic enhanced spectroscopic applications.

The angular variation of the electric field enhancement can be explained by the strength of the longitudinal bonding and antibonding plasmon modes of the Au NR dimer as a function of inter-rod angle. Shao *et al.* have shown that as the inter-rod angle increases, the longitudinal bonding mode becomes stronger while the antibonding mode weakens.[56] At an inter-rod angle of 180°, the LSPR of the NR dimers is exclusively due to the bonding plasmon mode, and the antibonding mode disappears (Fig. S8, ESI†). For side-to-side linked dimers, *i.e.*, at an angle of 0°, the longitudinal bonding mode becomes dark, and the LSPR of the NR dimer is dominated by the longitudinal antibonding mode (Fig. S8, ESI†). It is also known from the literature that when the NR dimers are excited resonantly at the bonding plasmon mode, light electric field enhancement is observed in the gap region.[56,65] However, when excited at the antibonding plasmon mode, no electric field enhancement is observed in the gap.[56] Therefore, as the angle between the arms of the NRs increases, the antibonding mode weakens, and the bonding mode strengthens, leading to an increasing enhancement of the light electric field.

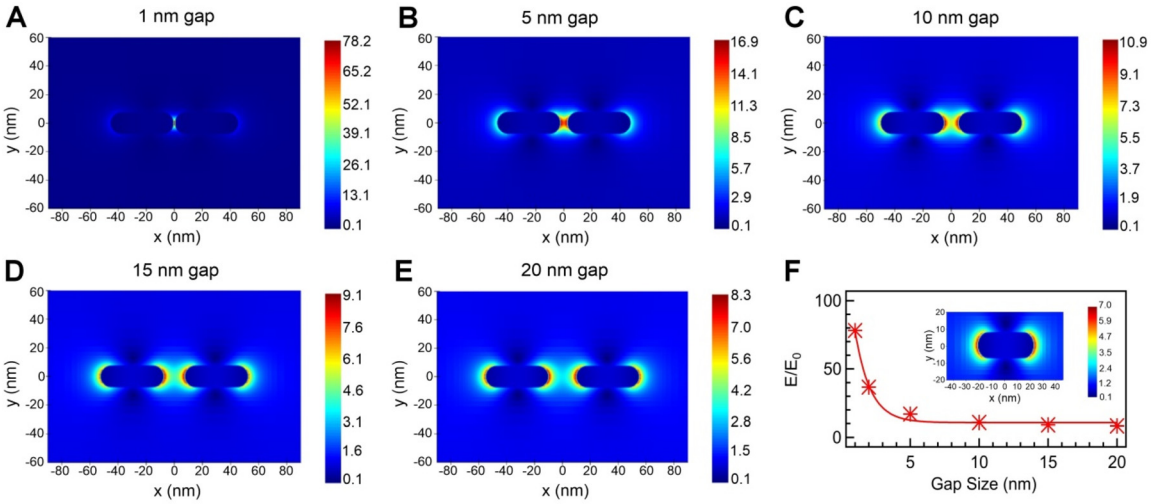

Fig. 7 Effect of gap size on the maximum electric field enhancement for Au NR dimers. (A) FDTD simulation results showing map of electric field enhancement for Au NR dimers at (A) 1 nm, (B) 5 nm, (C) 10 nm, (D) 15 nm, and (E) 20 nm gap size. (F) Plot of the electric field enhancement (E/E_0) of the Au NR dimers as a function of gap size. Inset shows the electric field distribution map for an Au NR monomer. Here, E_0 is the electric field in water in absence of any Au NR. E represents the maximum electric field at the gap between the two NRs. Light polarization is parallel to the *x* axis.

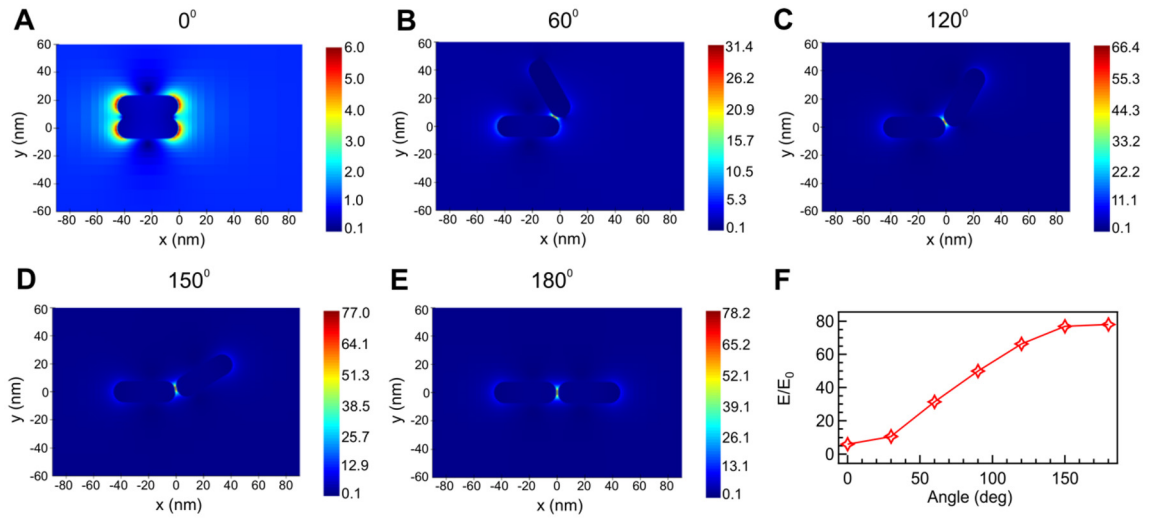

Fig. 8 Effect of angle between the Au NRs on the maximum electric field enhancement at the gap of the Au NR dimers. Map of the enhancement of the electric field (E/E_0) at (A) 0°, (B) 60°, (C) 120°, (D) 150°, and (E) 180°. (F) Plot of E/E_0 as a function of the angle between the Au NRs. Here, E represents the maximum electric field at the gap between the two NRs, while E_0 is the electric field in the absence of the Au NRs. The reference medium is water. Light polarization is along the *x* axis.

4. Conclusions

We have developed an easy and inexpensive method to synthesize end-to-end linked Au nanorod (NR) dimers in aqueous solution using 1,4-dithiothreitol (DTT) as a linker. The acid–base chemistry of DTT controls the assembly reaction, halting it at the dimer stage. At neutral and acidic pH, DTT is neutral and contains two thiol (–SH) groups, which anchor to two Au NRs, facilitating end-to-end coupling. At basic pH (pH > 11.0), both -SH groups of DTT deprotonate, making DTT dianionic. This dianionic DTT readily adsorbs onto the transverse surface of Au NRs, which is rich with positively charged CTAB micellar layers, preventing further binding with other NRs and stopping the reaction. We found that overall, 70% of the assembled structures are dimers, and over 90% of these are end-to-end linked with a gap distance of ~1 nm. These NR dimers exhibit exceptional stability, remaining intact for over two weeks. Finite difference time domain (FDTD) simulations show that the electric field enhancement in the gap region of these NR dimers is ~80 times higher than in a homogeneous water reference and 11 times higher than in Au NR monomers. Overall, we present a simple and cost-effective method to

prepare and control Au NR dimers with a gap distance of ~1 nm, which exhibit strong electric field enhancement in the gap region. This method will be useful in various applications such as high-resolution biosensing, chemical sensing, and photovoltaic devices.

Author contributions

S. Patra designed the experiments. S. Sharma and S. Pradhan were involved in the synthesis of Au nanorods. S. Sharma carried out all the optical and structural characterization studies. Q. Jiang and D. Gérard designed the FDTD simulation study, and T. Minchella performed the simulations. All authors discussed the results and contributed to the writing of the manuscript.

Data availability

The data supporting this article are provided within the main manuscript and in the ESI.†

Conflicts of interest

There are no conflicts to declare.

Acknowledgements

This study is supported by the start up research grant (SRG) from Science and Engineering Research Board (SERB), India (Project: SERB/SRG/2022/000341). The funding from research initiation grant (RIG) and additional competitive research grant (ACRG) of BITS-Pilani is also greatly acknowledged. S. S. acknowledges the JRF fellowship from SERB, India. T. M. acknowledges the PhD funding from Region Grand-Est as well as the Graduate School NANO-PHOT (Ecole Universitaire de Recherche, grant ANR-18-EURE-0013, France). S. Pradhan acknowledges institute fellowship from BITS-Pilani. We also acknowledge central research facilities of IIT Delhi and MNIT-Jaipur for providing access to use the TEM facilities.

References

1 G. P. Acuna, F. M. Möller, P. Holzmeister, S. Beater, B. Lalkens and P. Tinnefeld, *Science*, 2012, **338**, 506–510.
2 D. Punj, M. Mivelle, S. B. Moparthi, T. S. Van Zanten, H. Rigneault, N. F. van Hulst, M. F. Garcıa-Parajo and J. Wenger, *Nat. Nanotechnol.*, 2013, **8**, 512–516.
3 M. Dass, F. N. Gür, K. Kołątaj, M. J. Urban and T. Liedl, *J. Phys. Chem. C*, 2021, **125**, 5969–5981.
4 J. N. Anker, W. P. Hall, O. Lyandres, N. C. Shah, J. Zhao and R. P. Van Duyne, *Nat. Mater.*, 2009, **7**, 308–319.
5 P. Holzmeister, G. P. Acuna, D. Grohmann and P. Tinnefeld, *Chem. Soc. Rev.*, 2014, **43**, 1014–1028.
6 G. Baffou and R. Quidant, *Chem. Soc. Rev.*, 2014, **43**, 3898–3907.
7 S. Caprasecca, S. Corni and B. Mennucci, *Chem. Sci.*, 2018, **9**, 6219–6227.
8 E. Mauriz, P. Dey and L. M. Lechuga, *Analyst*, 2019, **144**, 7105–7129.
9 I. Tijunelyte, E. Guenin, N. Lidgi-Guigui, F. Colas, J. Ibrahim, T. Toury and M. Lamy De La Chapelle, *Nanoscale*, 2016, **8**, 7105–7112.
10 Q. Jiang, J. B. Claude and J. Wenger, *Nanoscale*, 2021, **13**, 4188–4194.
11 M. K. Veedu, J. Osmólska, A. Hajda, J. Olesiak-Bańska and J. Wenger, *Nanoscale Adv.*, 2023, **6**, 570–577.
12 E. C. Dreaden, A. M. Alkilany, X. Huang, C. J. Murphy and M. A. El-Sayed, *Chem. Soc. Rev.*, 2012, **41**, 2740–2779.
13 H. Altug, S. H. Oh, S. A. Maier and J. Homola, *Nat. Nanotechnol.*, 2022, **17**, 5–16.
14 V. Kaur, C. Kaur and T. Sen, *J. Phys. Chem. C*, 2023, **127**, 7308–7318.
15 O. Neumann, J. Zhou, Y. Ju, M. M. Bajomo, A. B. Sánchez-Alvarado, J. Dolive, B. Kumela, M. Kumela, A. Patel, P. Nordlander and N. J. Halas, *J. Phys. Chem. C*, 2024, **128**, 8649–8659.
16 S. Lal, S. Link and N. J. Halas, *Nat. Photonics*, 2007, **1**, 641–648.
17 V. Glembockyte, L. Grabenhorst, K. Trofymchuk and P. Tinnefeld, *Acc. Chem. Res.*, 2021, **54**, 3338–3348.
18 A. Kinkhabwala, Z. Yu, S. Fan, Y. Avlasevich, K. Müllen and W. E. Moerner, *Nat. Photonics*, 2009, **3**, 654–657.
19 L. Grabenhorst, F. Sturzenegger, M. Hasler, B. Schuler and P. Tinnefeld, *J. Am. Chem. Soc.*, 2024, **146**, 3539–3544.
20 S. Khatua, P. M. R. Paulo, H. Yuan, A. Gupta, P. Zijlstra and M. Orrit, *ACS Nano*, 2014, **8**, 4440–4449.
21 D. Punj, P. Ghenuche, S. B. Moparthi, J. de Torres, V. Grigoriev, H. Rigneault and J. Wenger, *Wiley Interdiscip. Rev.: Nanomed. Nanobiotechnol.*, 2014, **6**, 268–282.
22 M. F. Nüesch, M. T. Ivanović, J. B. Claude, D. Nettels, R. B. Best, J. Wenger and B. Schuler, *J. Am. Chem. Soc.*, 2022, **144**, 52–56.
23 N. J. Halas, S. Lal, W. S. Chang, S. Link and P. Nordlander, *Chem. Rev.*, 2011, **111**, 3913–3961.
24 R. Gill, L. Tian, W. R. C. Somerville, E. C. Le Ru, H. Van Amerongen and V. Subramaniam, *J. Phys. Chem. C*, 2012, **116**, 16687–16693.
25 Y. Zhang, B. Walkenfort, J. H. Yoon, S. Schlücker and W. Xie, *Phys. Chem. Chem. Phys.*, 2014, **17**, 21120–21126.
26 G. P. Acuna, F. M. Möller, P. Holzmeister, S. Beater, B. Lalkens and P. Tinnefeld, *Science*, 2012, **338**, 506–510.
27 E. Prodan, C. Radloff, N. J. Halas and P. Nordlander, *Science*, 2003, **302**, 419–422.
28 P. Biagioni, J. S. Huang and B. Hecht, *Rep. Prog. Phys.*, 2012, **75**, 024402.
29 B. Willingham, D. W. Brandl and P. Nordlander, *Appl. Phys. B: Lasers Opt.*, 2008, **93**, 209–216.

30 D. Punj, M. Mivelle, S. B. Moparthi, T. S. Van Zanten, H. Rigneault, N. van Hulst, M. F. García and J. Wenger, *Nat. Nanotechnol.*, 2013, **8**, 512–516.
31 S. Lee, Q. Zhao, S. Lee, M. N. Haddadnezhad, I. Jung and S. Park, *J. Phys. Chem. C*, 2024, **128**, 7202–7210.
32 M. Agio, *Nanoscale*, 2012, **4**, 692–706.
33 L. Scarabelli, A. Sánchez-Iglesias, J. Pérez-Juste and L. M. Liz-Marzán, *J. Phys. Chem. Lett.*, 2015, **6**, 4270–4279.
34 L. Liz-marzán, *Colloidal Synthesis of Plasmonic Nanometals*, CRC Press, 2020.
35 B. Nikoobakht and M. A. El-Sayed, *Chem. Mater.*, 2003, **15**, 1957–1962.
36 N. R. Jana, L. Gearheart and C. J. Murphy, *J. Phys. Chem. B*, 2001, **105**, 4065–4067.
37 T. K. Sau and C. J. Murphy, *Langmuir*, 2004, **20**, 6414–6420.
38 A. Kar, V. Thambi, D. Paital and S. Khatua, *Nanoscale Adv.*, 2020, **2**, 2688–2692.
39 X. Lu, D. Punj and M. Orrit, *Nano Lett.*, 2022, **22**, 4215–4222.
40 T. Zhang, N. Gao, S. Li, M. J. Lang and Q. H. Xu, *J. Phys. Chem. Lett.*, 2015, **6**, 2043–2049.
41 T. G. Habteyes, S. Dhuey, E. Wood, D. Gargas, S. Cabrini, P. J. Schuck, A. P. Alivisatos and S. R. Leone, *ACS Nano*, 2012, **6**, 5702–5709.
42 S. E. Lohse and C. J. Murphy, *Chem. Mater.*, 2013, **25**, 1250–1261.
43 C. J. Murphy, T. K. Sau, A. M. Gole, C. J. Orendorff, J. Gao, L. Gou, S. E. Hunyadi and T. Li, *J. Phys. Chem. B*, 2005, **109**, 13857–13870.
44 T. Jain, F. Westerlund, E. Johnson, K. Moth-poulsen and T. Bjørnholm, *ACS Nano*, 2009, **3**, 828–834.
45 K. K. Caswell, J. N. Wilson, U. H. F. Bunz and C. J. Murphy, *J. Am. Chem. Soc.*, 2003, **125**, 13914–13915.
46 P. Pramod and K. G. Thomas, *Adv. Mater.*, 2008, **20**, 4300–4305.
47 S. T. S. Joseph, B. I. Ipe, P. Pramod and K. George Thomas, *J. Phys. Chem. B*, 2006, **110**, 150–157.
48 J. Liu, C. Kan, Y. Li, H. Xu, Y. Ni and D. Shi, *Appl. Phys. Lett.*, 2014, **104**, 253105.
49 N. Hemant, A. Rahman, P. Sharma, A. Shanavas and P. P. Neelakandan, *Nanoscale*, 2024, **16**, 12127–12133.
50 K. Trofymchuk, K. Kołątaj, V. Glembockyte, F. Zhu, G. P. Acuna, T. Liedl and P. Tinnefeld, *ACS Nano*, 2023, **17**, 1327–1334.
51 W. Liu, L. Li, S. Yang, J. Gao and R. Wang, *Chem. – Eur. J.*, 2017, **23**, 14177–14181.
52 P. Zhan, P. K. Dutta, P. Wang, G. Song, M. Dai, S. X. Zhao, Z. G. Wang, P. Yin, W. Zhang, B. Ding and Y. Ke, *ACS Nano*, 2017, **11**, 1172–1179.
53 Y. Liu, Y. Liu and Y. Shen, *Int. J. Intell. Rob. Appl.*, 2018, **2**, 445–453.
54 X. Lu, D. Punj and M. Orrit, *RSC Adv.*, 2022, **12**, 13464–13471.
55 D. Nepal, K. Park and R. A. Vaia, *Small*, 2012, **8**, 1013–1020.
56 L. Shao, K. C. Woo, H. Chen, Z. Jin, J. Wang and H. Q. Lin, *ACS Nano*, 2010, **4**, 3053–3062.
57 I. Haidar, J. Aubard, G. Lévi, S. Lau-Truong, L. Mouton, D. R. Neuville, N. Félidj and L. Boubekeur-Lecaque, *J. Phys. Chem. C*, 2015, **119**, 23149–23158.
58 I. Haidar, G. Lévi, L. Mouton, J. Aubard, J. Grand, S. Lau-Truong, D. R. Neuville, N. Félidj and L. Boubekeur-Lecaque, *Phys. Chem. Chem. Phys.*, 2016, **18**, 32272–32280.
59 A. Hohenau, M. Bugnet, V. Kapetanovic, G. Radtke, G. A. Botton, N. Reichelt, U. Hohenester, J. R. Krenn, L. Boubekeur-Lecaque and N. Félidj, *Adv. Opt. Mater.*, 2024, **2400929**, 1–8.
60 A. F. Stewart, A. Lee, A. Ahmed, S. Ip, E. Kumacheva and G. C. Walker, *ACS Nano*, 2014, **8**, 5462–5467.
61 L. Novotny and B. Hecht, *Principles of Nano-Optics*, Cambridge University Press, Cambridge, 2006.
62 A. Kar, V. Thambi, D. Paital, G. Joshi and S. Khatua, *Langmuir*, 2020, **36**, 9894–9899.
63 A. Kar, M. Singh, D. Paital and S. Khatua, *J. Phys. Chem. C*, 2021, **125**, 23895–23903.
64 D. H. Tsai, T. J. Cho, F. W. Delrio, J. M. Gorham, J. Zheng, J. Tan, M. R. Zachariah and V. A. Hackley, *Langmuir*, 2014, **30**, 3397–3405.
65 J. Kumar, X. Wei, S. Barrow, A. M. Funston, K. G. Thomas and P. Mulvaney, *Phys. Chem. Chem. Phys.*, 2013, **15**, 4258–4264.
66 N. Suwandaratne, J. Hu, K. Siriwardana, M. Gadogbe and D. Zhang, *Anal. Chem.*, 2016, **88**, 3624–3631.
67 P. K. Jain, S. Eustis and M. A. El-Sayed, *J. Phys. Chem. B*, 2006, **110**, 18243–18253.
68 C. Tabor, D. Van Haute and M. A. El-Sayed, *ACS Nano*, 2009, **3**, 3670–3678.

